IAC–18–A3.4A.8

Binary asteroid redirection: science opportunity for nanosats

Andrea Capannolo
Politecnico di Milano, Italy
andrea.capannolo@polimi.it

Vincenzo Pesce
Politecnico di Milano, Italy
vincenzo.pesce@polimi.it

Michèle Lavagna
Politecnico di Milano, Italy
michelle.lavagna@polimi.it

Although just few tens of binary asteroid systems are known, still they represent an intriguing natural facility for both planetary and universe science further understanding and technology in orbit demonstration. In particular, one of those, the Didymos system, recently captured the space community interest as a perfect target to test capabilities in detecting natural objects, for planetary protection. Indeed, JHU/APL, supported by NASA, are designing the Double Asteroid Redirection Test (DART) mission to impact on the Didymos secondary moon (Didymos B), and assess the kinetic impactor strategy performance to deflect a 150 m wide small asteroid. The impact ejecta, being DART a single spacecraft mission, will be monitored only remotely from Earth. However, to possibly be in close view of the impact point just before and after the kinetic event occurrence would offer the chance to collect unique scientific data: potential fragmentation of Didymos B could be registered, and plume material in situ analyzed. A simple plume evolution imaging may even offer fundamental information on the natural bodies composition and the deflection effectiveness. Assuming the possibility for the main spacecraft to host a small piggyback nanosat, the paper assesses the science opportunities offered by releasing the nanosat at the Didymos system arrival, to witness the impact and post-impact events in the Didymos B proximity. The time-to-impact nanosat release, the release relative velocity direction and magnitude are assumed as degrees of freedom to generate families of trajectories to maximize the post-impact environment monitoring, under the multi-body gravitational field of the binary system. The effectiveness of a low authority on board propulsion unit is also considered to widen the trade space for the nanosat trajectories in the binary proximity which maximize the time of residence in the impact region vicinity. Analyses showed that the nanosat trajectory can be tuned so that the impact expected fragments can be imaged from different perspectives, making the piggyback nanosat a very interesting added value to the kinetic impactor mission. The paper synthesizes the different opportunities that the proposed piggyback cubesat offers if the limited engineering and operational degrees of freedom merged with the peculiar gravity field are carefully exploited.

1. Introduction

Asteroid deflection is nowadays a topic of great interest in the space community. The DART (Double Asteroid Redirection Test) mission will open the way to a new set of missions aimed at assessing the effectiveness of currently existing techniques for planetary deflection [1]. The NASA's spacecraft will impact the small moon of the Didymos binary system (Didymos B), changing its orbit with respect to the main attractor (Didymos A). Also, particles ejected from the crater and their evolution in time would provide data about the gravitational environment and internal asteroids composition. All these measurements are based on ground observations [2]. By exploiting the available mass in DART spacecraft for more payload, a CubeSat can be used observe the impact, the ejecta, and the binary system in general, from a close distance. Given the low performance capabilities of a CubeSat, and the constraint of DART trajectory and velocity [3,4], it is fundamental to design a suitable trajectory, based on simplicity of operations, which would allow the CubeSat to fly at close distance from the system, while being able to avoid

the impact with the asteroid and the ejecta coming from the crater. In this frame, the paper presents the process of selection of the most suitable flybys to fulfill these requirements. After a definition of the low level objectives that the mission has to satisfy, a map of trajectories is computed from a set of release directions from DART spacecraft. Then, each parameter considered for the selection is evaluated as a function of design parameters, and some observations are drawn. Finally, optimal trajectories are defined, their properties are discussed and the robustness to release and thrust variables is assessed.

2. Mission overview

The CubeSat is designed for being docked to DART spacecraft and detached before the impact with Didymos B, to provide additional scientific data from the observation of the impact, of the evolution of the impact ejecta, and of the impact crater. To fulfill these requirements, few design drivers must be taken into account:

- To visualize the impact, the CubeSat shall be at a distance suitable for imaging (based on camera performance)
- To track the evolution of ejecta and allow crater visibility, the CubeSat arrival to the system shall be delayed to allow sufficient time for the dust to expand

For these reasons, the study is performed with particular attention on the minimization of distances and maximization of time windows.

2.1 Design criteria and parameters

According to the "short distance, long time" philosophy, the criteria to be fulfilled for the design have been developed in detail:

- Minimization of the CubeSat distance from the system during the impact
- Minimization of the Cubesat distance during the passage near the impact site
- Maximization of the observability time of the binary system
- Maximization of the time delay to reach the passage near the impact site
- Minimization of rotation rate (to reduce the pointing burden to the ADCS system of the CubeSat)

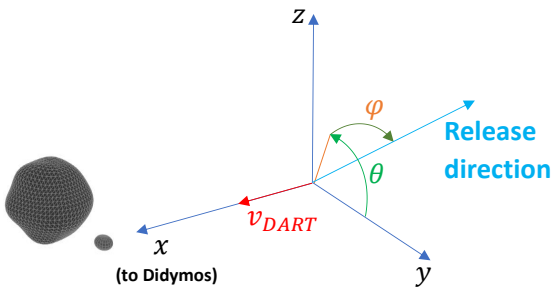

Figure 1: Release angles

To explore the set of possible trajectories and define the most suitable, according to the listed criteria, parameters describing the time and the direction of the CubeSat release are considered:

- Release time ($T_{release}$): instant when the CubeSat is undocked from DART spacecraft.
- Release latitude angle (φ): angle describing the release component along DART spacecraft's velocity direction
- Release longitude angle (θ): angle describing the release component normal to DART spacecraft's velocity

For sake of clarity, the two release angles are depicted in Figure 1. The latitude angle extends from -90° (release coincident with DART spacecraft velocity) to 90° (release opposite to DART spacecraft velocity). The longitude angle covers all possible direction in the normal plane. In particular, 0° corresponds to a release on Didymos orbital plane, towards the left of the system; 90° points above the system; 180° points the left; 360° points below the asteroids. In addition, some other fixed parameters have been introduced to make the simulation compliant with the mission planning and spacecraft performances. These parameters are:

- T_{undock}: time window between release and engine ignition
- Δv_{undock}: release speed from the docking system
- Δt_{burn}: time required for the engine to burn all the propellant
- F_{burn}: average thrust level provided by the engine

2.2 Scenarios

Given the parameters introduced in section 2.1, the design is still unconstrained in terms of the CubeSat thrust direction. This degree of freedom gives the possibility to develop a virtually infinite set of trajectories, however, following the scope of this study, the two extreme scenarios have been taken into account:

- "Radial thrust": the release Δv and the thrust are in the same direction, thus making the CubeSat depart from DART spacecraft radially; this creates a partial lateral deviation plus a braking component (depending on the angles).

- "Backward thrust": the thrust is always directed backwards with respect to DART spacecraft velocity, thus the lateral deviation is given by the undocking mechanism only; this creates a small lateral deviation and a full braking action of the CubeSat.

The two scenarios serve as baseline for future studies on hybrid approaches, where different maneuvers may be exploited during the departure.

2.3 Target model

The whole simulations are performed in a synodic reference frame, considering the effect of both asteroids on the CubeSat's trajectory. The distance between the two bodies is assumed to be constant, therefore the dynamics environment is the Circular Restricted Three Body Problem (CRTBP) [5]. Although the irregular shape of the bodies would cause small perturbations on the trajectories, the characteristic times of the flyby are so small that a point mass model represents a very good approximation. The exact shape of the attractors can be used in the future to study the evolution of the low energy ejecta after the impact, that will be captured by the binary system's gravity. The long permanence around the system will make the irregular shape effect visible, therefore the study of the ejecta evolution will require more refined model, such that polyhedral shapes of the asteroids [6–9]

3. Trajectories analysis and selection

The computation and study of the possible trajectories has been carried out for the two scenarios in parallel. To make a comparative analysis, every step of the study is presented for both cases, paying attention to the main differences between approaches.

3.1 Parameters values and model assumptions

The set of values for the design variables are reported below:

- $T_{release} = [2, 4, 10, 24, 36, 120]\, h$ (time before impact);
- $T_{undock} = 30\, min$;
- $\Delta t_{burn} = 7830\, s$;
- $F_{burn} = 0,1\, N$;
- $\theta = 0° \rightarrow 360°$,10° step;
- $\varphi = 0° \rightarrow 90°$,1° step;

Some assumptions are introduced in the model for the whole study, to provide preliminary trajectories, to be refined in the next phases of the overall mission design. In particular:

- DART trajectory
  - DART spacecraft trajectory is approximated as a straight line from the CubeSat release instant to the impact with Didymos B
  - DART spacecraft impacts Didymos B at exactly 90° with the asteroid's surface
- Environment properties
  - No solar perturbation
  - Sun located at 60° from the zenith of the impact site, on Didymos's orbital plane
  - Orbital planes of Didymos B around Didymos A, and of Didymos system around the Sun, are coincident (Sun always on asteroids' equator)
  - Didymos B orbit around Didymos A at constant distance (1180 m)
- Camera properties
  - Maximum distance for observation: 500 km
  - Camera Field of View: 4.1°
  - Resolution of 1 m/px below 70 km distance
- Safety
  - Minimum distance from the impact site: 15 km

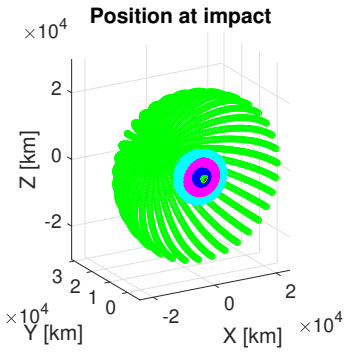

(a) 3D view

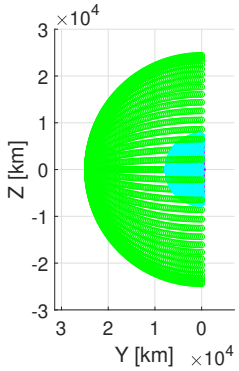

(b) Y-Z plane projection

Figure 2: CubeSat positions at DART impact as function of release direction and time (Radial thrust)

3.2 Range analysis

Trajectories are propagated (coherently with the design variables set) until DART spacecraft impacts, to map the range of positions of the CubeSat when the observation of the impact starts. Then, distance from the binary system's center of mass is evaluated, to verify the visibility of the event. Finally, the minimum distance from the impact site is computed, to understand the level of resolution achievable with the camera.

Radial thrust

The ranges achieved by the CubeSat are strongly dependent on the latitude angle and the release time: while the release time influences the axial distance from the binary system, the angle contributes to enlarge both axial distance (minimally) and lateral shift of the CubeSat. The latter is proportional to the instant of release (see Figure 2). The space reachable by the CubeSat (at DART impact) is a spherical cap

$T_{release}$ $[h]$	$Distance\ (Axial = Lateral)$ $[km]$
120	24440
36	7182
24	4716
10	1840
4	608
2	197

Table 1: Max lateral and axial shift of CubeSat from Didymos, at DART impact (Radial thrust)

with dimensions proportional to the time of release. Table 1 reports main dimensions of the caps.

Because of the spherical shape of CubeSat final positions, the modulus of the distance is constant and equal to the maximum value of axial shift from Table 1. The most effective parameter to reach specified distance from the system at DART impact is the release time, while the latitude angle allows to introduce lateral shifts. Furthermore, reported values suggest that the only option for imaging the impact event (within acceptable resolution of the camera) is the latest release (2 h).

The minimum distance from impact site is reached at different times as the release time changes, however, the only driver for its value is the latitude angle. In fact, the tuning of the latter allows to increase lateral shifts (at the cost of lower braking action). The results show that tuning properly the latitude angle may greatly affect the quality of the observation. Also, it is observed that the CubeSat is able to reach the edge of the visibility sphere for any deployment time except the latest one (2 hours before impact), where it reaches 196 km.

Backward thrust

In this scenario, the latitude angle is effective to the trajectory only through the Δv provided by the release mechanism ($1.14\,m/s$), therefore its effect is significantly smaller. The distances at impact are comparable to the radial thrust case when the release latitude angle is close to $90°$, since the radial thrust profile approaches the backward one. The largest difference is observed at low latitude angles: due to the small contribute of the release mechanism, the lateral shift is significantly lower than in the radial thrust scenario. Consequently, the space reached by the CubeSat is characterized by almost flat circles at an

$T_{release}$ $[h]$	*Distance* $[km]$	
	Axial	*Lateral*
120	24440	496
36	7182	151
24	4716	102
10	1840	44
4	608	20
2	197	11

Table 2: Max lateral and axial shift of CubeSat from Didymos, at DART impact (Backward thrust)

$T_{release}$ $[h]$	*Maximum Distance* $[km]$
$120h$	500
$36h$	151
$24h$	101.6
$10h$	43.5
$4h$	18.6
$2h$	10.3

Table 3: Maximum distance of CubeSat from impact site (Backward thrust)

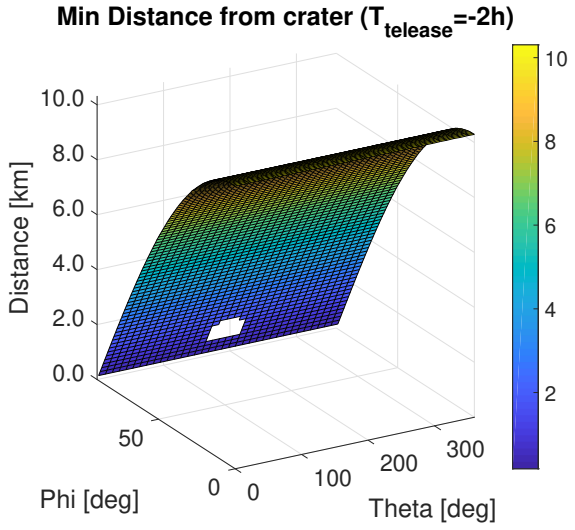

Figure 3: CubeSat minimum distances from crater (Backward thrust)

axial distance from the system comparable to the one from previous scenario, but with smaller radii.Values of axial and lateral shifts are reported in Table 2.

The small lateral shifts at impact cause also very close passages by the asteroid. In fact, distances are sufficiently small to make the CubeSat crash in some release conditions (see Figure 3). The holes in the surface represent crash conditions with Didymos asteroids (A or B).

The values for maximum distances are reported in table 3.

3.3 Time windows analysis

Among the whole set of trajectories developed and analyzed in section 3.2, the ones whose minimum distance from the binary system is above 500 km are discarded, since the camera would not allow a sufficiently satisfactory imaging. The remaining solutions are all potentially suitable for the final design, however, to maximize the scientific return, a study on the timing for observation is required. In particular, two main data are taken into account, as explained in Section 2.1: the time delay to reach minimum distance, and the time spent below 500 km around the system. The first parameter is a direct measurement of the time of evolution for the ejecta of the impact that can be tracked by the CubeSat; the second parameter indicates the level of evolution of the ejecta when the resolution of the images is the highest: the higher the delay, the more spread the ejecta cloud, the higher the chances of imaging the particles and observing the impact crater below the cloud. The analysis takes also into account the obscuration effects that may arise from both the Sun (dazzle) and Didymos A (eclipse), which may undermine the results of the support of the CubeSat. With reference to Figure 4, recalling the Sun angle and Didymos B orbit radius from Section 3.1, define:

- $\underline{l}_{dD}$: position vector from Didymos B to Didymos A
- $\underline{l}_{Cd}$: position vector from CubeSat to Didymos B
- $\underline{l}_{CS}$: position vector from CubeSat to Sun

These vectors are exploited to evaluate the two visibility angles, namely θ_D (angle between Didymos A and the CubeSat, centered in Didymos B) and θ_S (angle between Didymos B and the Sun, centered in the CubeSat). To avoid Sun dazzle, θ_S must be greater or equal to half of the camera FoV, while to avoid eclipse, Didymos B must be in sight, therefore θ_D must be greater or equal than the eclipse angle

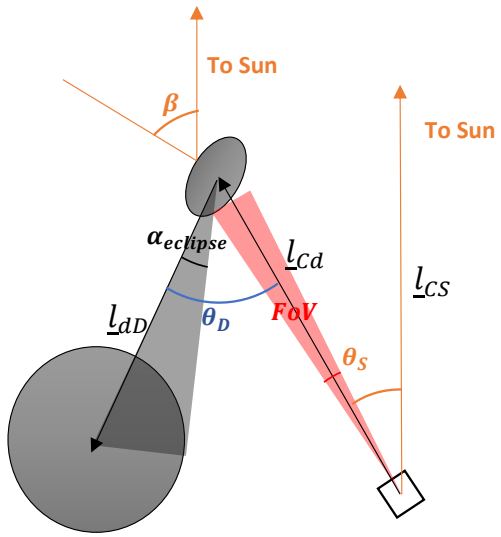

Figure 4: Visibility angles

$\alpha_{eclipse}$, defined as:

$$\alpha_{eclipse} = \arcsin\left(\frac{R \cdot w}{\|\underline{l}_{dD}\|}\right) \tag{1}$$

with R being the maximum radius of Didymos A and w a weight to increase the radius value by 20% (to ensure a good visibility). Since the distance between the asteroids is assumed constant, the threshold angle $\alpha_{eclipse}$ is constant as well, and equal to 24.64° .

As already mentioned in section 3.1, an inclination of 60° between the Sun direction and the impact site surface normal is assumed. All time intervals in which eclipse or dazzle are present are removed from the time count for observation.

Radial thrust

The map of observation times for the three release times scenarios highlighted some common features:

- The release longitude angle (θ) is relevant only when around 180° , since the passage on the right of the system (behind Didymos A) causes the eclipse of Didymos B. In all other cases, the time variations are negligible.
- Sun dazzle is present when θ is around 180° .
- The total visibility time is proportional to the latitude angle φ

On the other hand, some differences are present:

- The earlier the release, the higher the dependence on the release angle φ, due to the increased distance from the center of the observability sphere
- A release of more than 4 hours earlier than the impact time does not add extra time for observation

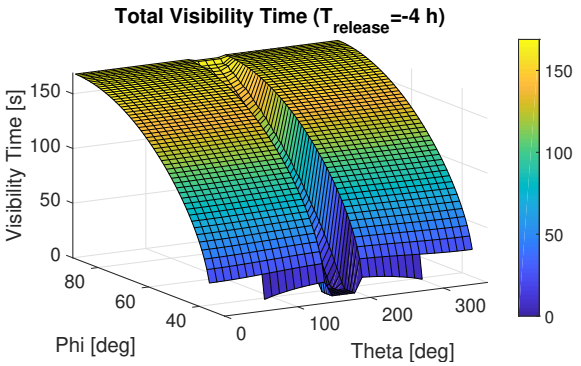

Figure 5: Total visibility time for intermediate release (Radial thrust)

The last feature is the most interesting one, because it means that from the release at 4 hours the longest possible visibility time (around 169 seconds) is achieved, hence the choice of the best release time between late and intermediate release shall be made according to the other criteria. The release at 2 hours, instead, displays a maximum time of 117 seconds.

As an example, Figure 5 depicts the trend of the visibility time, where it is possible to observe the effect of the eclipse (visibility time drop in the middle of the plot) .

Regarding the delay time, no boundary is present and the value gets higher as the release is anticipated. Therefore, the early release represents the best solution in that sense. Table 4 reports maxima and minima of the delay time for each release scenario.

Notice that the earlier the release, the higher the maximum delay achievable, but also the smaller the range of possible delays (due to the reduced range of angles allowed to ensure minimum distances below 500 km).

Backward thrust

All observations made for the radial thrust profile are still valid for the axial case, except the dependence of time on the release latitude angle φ: in fact, its variation does not influence (in a relevant fashion) the overall time, being the angle related on the release action only, and decoupled from the thrust. This generates nearly constant values, regardless of release an-

Time Delay [s]		
$T_{release}$	Min	Max
$120h$	4126	4129
$36h$	1209	1214
$24h$	787	797
$10h$	294	311
$4h$	54	102
$2h$	0	33

Table 4: Time delay from release to reach minimum distance (Radial thrust)

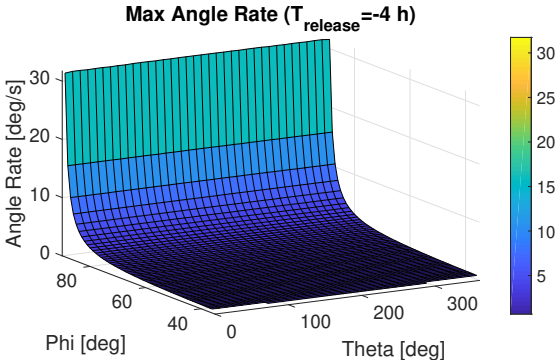

Figure 6: Maximum rotation rate for intermediate release (Radial thrust)

Time Delay [s]		
$T_{release}$	Min	Max
$120h$	4042	4129
$36h$	1187	1213
$24h$	779	797
$10h$	303	311
$4h$	99	103
$2h$	31	33

Table 5: Time delay from release to reach minimum distance (Backward thrust)

Rotation Rate [deg/s]		
$T_{release}$	Min	Max
$120h$	0.78	0.78
$36h$	0.9	2.69
$24h$	0.69	4.09
$10h$	0.71	10.5
$4h$	0.7	31.73
$2h$	1.76	98.4

Table 6: Max and min of angular rate peaks for each release time (Radial thrust)

gles (exception made for the eclipse event), which are equal to maximum values from the radial thrust scenario (117-118 seconds for the release 2 hours before impact, 169 seconds for earlier deployments).

The delay time has values comparable with the maxima found for radial thrust profile (because the two model are similar at high φ releases). Regarding minimum values, backward thrust would always have higher delay times, however, due to the lower range of available angles for Radial thrust, early release minimum delays are higher in the esrly deployments. See Table 5 for details.

3.4 Pointing analysis

Close flybys are preferred for better imaging, however, very short distances would be an excessive burden for the CubeSat attitude control subsystem, to ensure constant pointing for the whole trajectory. To assess peaks in the attitude rotation rate and acceleration, position vector (from Didymos CoM) and CubeSat velocity vector are mapped for each trajectory. Then the angle between the vectors (the pointing angle) and its derivatives are evaluated. The peak of the angular rate, which is reached at the closest distance from the system, is mapped for all release angles.

Radial thrust

The advantage of a radial thrust profile (in terms of CubeSat pointing) is the longer distance achievable from the system. The direct consequence is a steep drop of the angular rate as the latitude release angle decreases (see Figure 6). Therefore, to reduce the burden to the attitude control system, it is enough to avoid highest latitude angles (87° - 90°), specially for late deployments.

Table 6 reports the maximum and minimum values for the angular rate at each release time.

Time Rotation rate $[deg/s]$		
$T_{release}$	Min	Max
$120h$	0.68	40.06
$36h$	2.25	185.1
$24h$	3.35	193.4
$10h$	7.81	449.6
$4h$	18.24	1050
$2h$	32.94	1889

Table 7: Max and min of angular rate peaks for each release time (Axial thrust)

Backward thrust

The axial thrust profile is characterized by closer flybys to Didymos system. The direct consequence is a higher control effort to maintain the constant pointing for observation. In fact, the all values are one or two orders of magnitude higher than the radial thrust case.

Table 7 reports the maximum and minimum values for the angular rate at each release time.

3.5 Optimal trajectories search

The selection of the optimal trajectory takes into account all criteria previously discussed, therefore it is posed as a multi-objective optimization problem. However, most of the criteria considered are related to each other, and in general the objective is to find the most balanced solution. For these reasons, the multiple objectives are converted to a single objective by an equally weighted summation of all criteria, to define the overall cost function "J":

$$J = J_D + J_d + J_{\Delta t} + J_{t_{delay}} + J_\omega \qquad (2)$$

where each element is scaled from one to zero according to the maximum and minimum values among all trajectories. Finally, the overall value of J is again scaled to obtain a value between zero and one.

The cost J is evaluated separately for each release time, to determine the best option for each release instant. The solutions whose minimum distance is below 15 km are directly discarded, to take into account possible uncertainties in the navigation.

The surface of the cost behavior as a function of release angles is a combination of all the trends of previous criteria, as shown in Figure 7.

As a consequence, it is possible to identify a crest on the surface where the maximum value is reached.

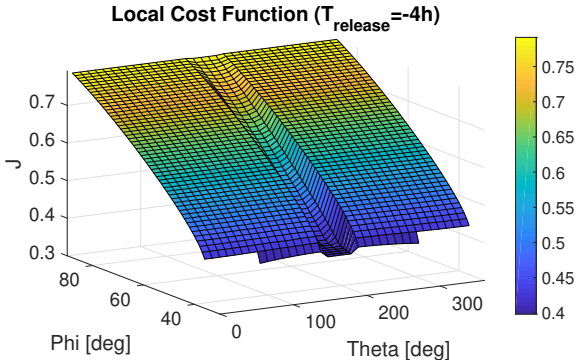

Figure 7: Cost function for intermediate release (Radial thrust)

$T_{release}$ $[h]$	θ $[deg]$	φ $[deg]$
-2	62	85
-4	206	87
-10	206	89
-24	0	89
-36	0	89
-120	144	89

Table 8: Optimal release parameters for each release time (Radial thrust)

Notice also than the angle θ does not affect the height of the surface except in the central (eclipse) zone.

Table 8 and Table9 show the optimal design parameters for each thrust profile and release time, while Table 10 and Table 11 display the values of the single criteria corresponding to the optimal release parameters.

It is possible to notice some features:

- The radial thrust optimal solutions have release angle φ which increases as the deployment is anticipated
- Backward thrust φ angle is much lower because of the lower lateral shift effect
- The 2 hours release for backward thrust is not early enough to achieve the minimum acceptable distance.
- Radial thrust solutions have the minimum distance proportional to the initial distance, and inversely proportional to maximum attitude rotation

$T_{release}$ $[h]$	θ $[deg]$	φ $[deg]$
-2	$-$	$-$
-4	144	36
-10	134	69
-24	154	81
-36	206	84
-120	216	88

Table 9: Optimal release parameters for each release time (Backwards thrust)

- Release before the 4 hours solution does not add more time spent in the visibility sphere, but increase the delay for ejecta observation
- Backward thrust has initial distance similar to the radial thrust case, but minimum distance always close to the minimum value allowed
- Delay times for Backward thrust are comparable with the ones form radial thrust profile

Because of the rapid increase of minimum distance for the radial thrust scenario, the best options would be the intermediate-late deployments (4-10 hours before DART impacts). In the backward thrust scenario, instead, the only parameter affected by the release time is the delay time, therefore, to maximize it, early deployments would be suggested.

Nevertheless, if an analysis on the ejecta cone expansion is included in the assessment of most suitable trajectories, some modifications need to be introduced. To ensure safety for the flyby, the study considered the worst impact scenario, with a basalt-based surface for Didymos B, which causes the fastest ejection velocity of impact particles (peaks of 320-325 m/s). The model correlates the ejection velocity of the single particle to the distance from the center of the crater (with particles on the sides being slower than the ones from the center) [10–12]. As a result, the deployment time for the radial thrust profile should be limited to intermediate-late releases, while in the backward thrust profile, the release should be constrained to the very late deployments (to prevent ejecta from large expansions), otherwise the short distance would cause a high risk of particles impact (see Figure 10). The direct consequence of this selection is that a radial thrust profile would ensure a wide view of the overall binary system and ejecta cone, although a lower resolution would be achieved. On the contrary, the backward thrust profile is the best option for high quality imaging, but limited to the surroundings of the impact site. Figure 8 and Figure 9 display the characteristic dimensions of the two asteroids as seen by the camera during the close passage.

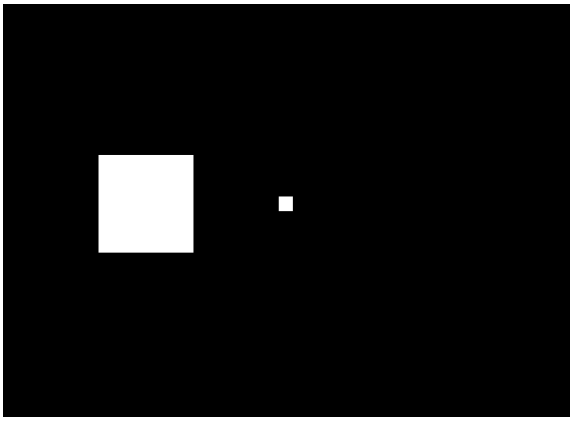

Figure 8: Didymos A and B dimensions as seen by the camera at close approach (Radial thrust)

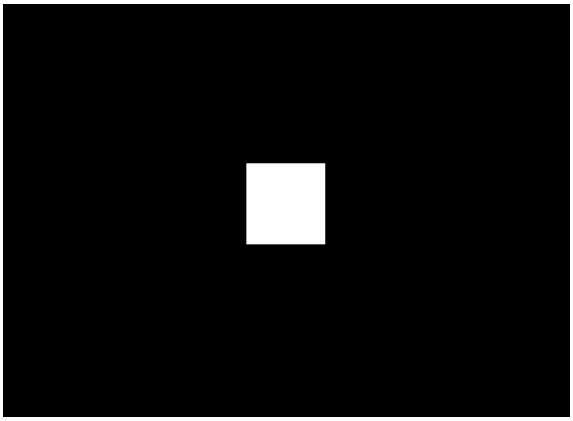

Figure 9: Didymos B dimensions as seen by the camera at close approach (Backward thrust)

3.6 Sensitivity analysis

To complete the assessment of suitable trajectories for the CubeSat flyby, a robustness against release and thrust uncertainties is necessary. To fulfill this task, a gaussian distribution is assumed for all release and thrust angles, and for the release time, while half gaussian is selected for the release and thrust Δv (since it is not possible to obtain a higher value than the maximum allowed by the engine). Table 12 resumes all standard deviations (1σ) for each parame-

$T_{release}$ $[h]$	D [km]	d [km]	δt [s]	t_{delay} [s]	ω [deg/s]	$\dot{\omega}$ $[deg/s^2]$
-2	195.6	17.2	117.4	33	19.70	2.19
-4	606.4	32.1	168.7	102.5	10.58	0.63
-10	1839.1	32.4	168.6	310.9	10.47	0.62
-24	4715.4	83.2	166.6	797.2	4	0.09
-36	7180.8	126.6	163.4	1213.7	2.53	0.04
-120	24438	430.4	86.4	4128.4	0.79	0.004

Table 10: Optimal objectives for each release time (Radial thrust)

$T_{release}$ $[h]$	D $[km]$	d $[km]$	δt $[s]$	t_{delay} $[s]$	ω $[deg/s]$	$\dot{\omega}$ $[deg/s^2]$
-2	–	–	–	–	–	–
-4	599	15	168.9	101.2	22.55	2.87
-10	1836.3	15.6	168.9	310.3	21.77	2.69
-24	4714.2	15.9	168.9	796.6	21.37	2.59
-36	7180	15.8	168.9	1213.2	21.49	2.61
-120	24438	17.2	168.9	4129.4	19.68	2.20

Table 11: Optimal objectives for each release time (Backward thrust)

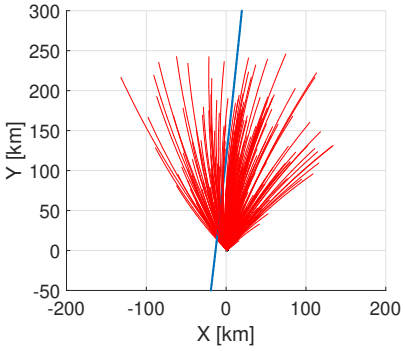

Figure 10: FlyBy trajectory intercepting the impact particles (Backward thrust)

ter. In addition, a 5km (1σ) uncertainty on DART s/c position with respect to Didymos is assumed.

Each design variable is perturbed according to the nominal value and its standard deviation, generating a mesh of 500 intial perturbed condition. Then, dynamics are propagated and final deviation of the CubeSat (in terms of distance from the binary System) is stored. This procedure is repeated for each design variable (maintaining the others at nominal value), to assess the sensitivity to the single parameter, and then for all parameters perturbed at the same time to have the real perturbed trajectories. From the results it is found that the most perturbing parameters are φ_{thrust} and Δv_{thrust}, while the others have a minimal effect. In fact, the probability density function of the completely perturbed initial condition is nearly the same as the one with the only φ_{thrust} perturbation.

The latitude angle release uncertainty causes large deviations of the trajectory, also proportionally to the release time anticipation. Figure 11 depicts the spread of possible distances achievable by the CubeSat depending on the release time.

The resulting trend is a gaussian distribution, with a spread of distance variation depending on the release. Uncertainty greatly affects the quality of the

$T_{release}$ $[s]$	$\Delta v_{release}$ $[m/s]$	$\theta_{release}$ $[deg]$	$\varphi_{release}$ $[deg]$	Δv_{thrust} $[m/s]$	θ_{thrust} $[deg]$	φ_{thrust} $[deg]$
10	0.14	5	5	0.56	1	1

Table 12: Standard deviation for all release and thrust design parameters

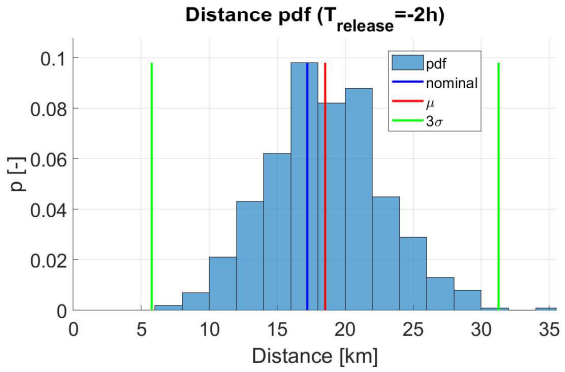

(a) Late release position uncertainty

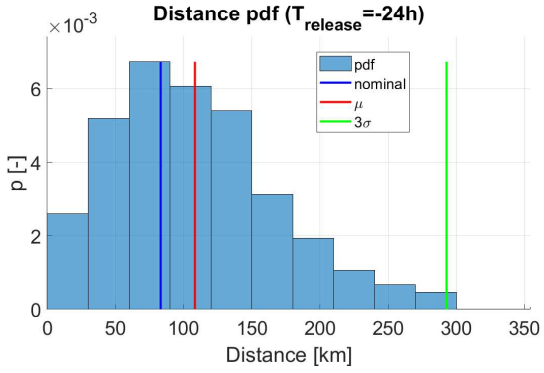

(b) Intermediate release position uncertainty

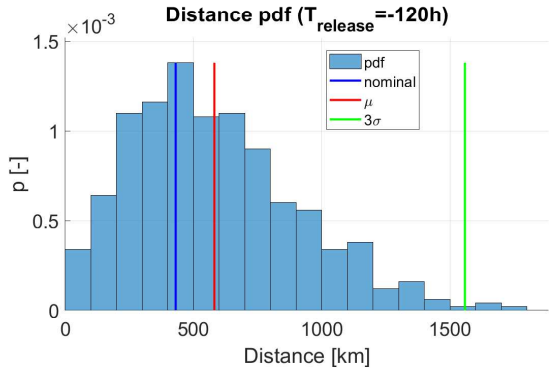

(c) Early release position uncertainty

Figure 11: CubeSat uncertainty of distance from the binary system (Radial thrust)

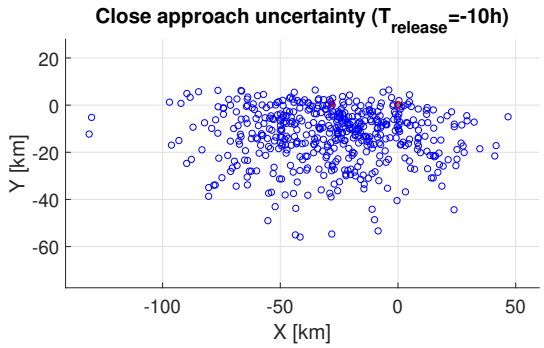

Figure 12: Close approach uncertainty cloud (Radial thrust)

imaging, thus requiring a better control of the trajectory (feedback control). Also, for intermediate deployments and earlier, the position of the CubeSat at close approach may fall on the other side of the binary system (as shown in Figure 12), thus potentially causing a failure in the asteroid identification and pointing.

While the radial thrust solutions partially compensate this deviation with nominal solutions that are farther from the system, the backward thrust scenario (which is subjected to the same level of uncertainty) does not guarantee safety during the passage, having its solutions high risks of impact with ejecta and large chances of approaching the system from the wrong side. To make the nominal trajectories robust to uncertainties, and ensure the success of the mission for the CubeSat, some changes in the deployment procedure should be introduces. Since the main cause of uncertainty is the thrust direction given by angle φ_{thrust}, it may be a solution to reduce the amount of Δv to be exploited by the CubeSat, at the cost of lower times to observe the asteroids system. If possible, part of the Δv could be restored by a small maneuver of DART spacecraft, which would ensure higher accuracy and would not affect the uncertainties in a relevant way. Other possible strategies can be the exploitation of a feedback (from DART

or ground) of the relative position of the CubeSat, in order to perform correction maneuvers before the flyby.

4. Conclusions

The paper addressed the feasibility of the exploitation of a small CubeSat as a support for the DART mission. The chance of observing the impact, the ejecta, and the crater from close distance would greatly enhance the science return of the overall mission. The scenario of a mission support exploiting a CubeSat has been analyzed according to different factors and criteria, such as the amount of time available to observe the system and the distances at which the impact becomes visible. This led to a set of suitable flybys, depending on the deployment time by DART spacecraft and on the thrust profile of the CubeSat. Then, the expansion of the ejecta cloud was taken into account to assess the safety of the previously selected flybys. The analysis showed that intermediate or late deployments (below 10 hours before the impact) ensure lower risks of hitting the impact particles. To reduce the chances to zero, it is necessary, for a radial thrust profile, to reach longer distances from the system (exploit higher lateral shifts from the main spacecraft), at the cost of a lower resolution for the observation. For the backward thrust scenario, the only viable solution is to deploy the CubeSat late, so that the ejecta won't expand enough during the short time available. Finally, robustness of the identified nominal trajectories is addressed, showing that the most influencing parameter for uncertainties is the thrust direction of the CubeSat. The result is a spread distribution of possible flybys, which may cause the failure of the mission due to high impact risks or approaches to the binary system from unexpected relative positions.

As future developments, the study will assess the amount of risk of hitting the particles when passing through the ejecta cloud, as a function of the particles distribution and size. Furthermore, the analysis on Δv will be carried on and possible uncertainties reduction versus mission effectiveness drops will be assessed. Secondly, the most suitable distances from the system to be achieved will be defined through simulations of the camera hardware, to verify the capability of visualizing the particles expansion and the crater beneath the cloud. Also, some strategies for reducing the burden to the attitude control system will be tested, such as letting the observed object image shift on the camera sensor to relax the constant pointing constraint. Finally, the chance of intercepting other asteroid systems after the flyby will be assessed, to maximize the exploitation of the CubeSat.

References

[1] A.F. Cheng, J. Atchison, B. Kantsiper, A.S. Rivkin, A. Stickle, C. Reed, A. Galvez, I. Carnelli, P. Michel, and S. Ulamec. Asteroid impact and deflection assessment mission. *Acta Astronautica*, 115(Supplement C):262 – 269, 2015.

[2] A.F. Cheng, P. Michel, M. Jutzi, A.S. Rivkin, A. Stickle, O. Barnouin, C. Ernst, J. Atchison, P. Pravec, and D.C. Richardson. Asteroid impact & deflection assessment mission: Kinetic impactor. *Planetary and Space Science*, 121(Supplement C):27 – 35, 2016.

[3] Bruno V Sarli, Martin T Ozimek, Justin A Atchison, Jacob A Englander, and Brent W Barbee. Nasa double asteroid redirection test (dart) trajectory validation and robutness. In *27th AAS/AIAA Space Flight Mechanics Meeting*, 2017.

[4] Martin T Ozimek and Justin A Atchison. Nasa double asteroid redirection test (dart) low-thrust trajectory concept. In *27th AAS/AIAA Space Flight Mechanics Meeting, San Antonio, USA*, volume 221, 2017.

[5] V Szebehely. *Theory of Orbits: The Restricted Problem of Three Bodies*. Academic Press, New York and London, 1967.

[6] R A Werner and D J Scheeres. Exterior gravitation of a polyhedron derived and compared with harmonic and mascon gravitation representations of asteroid 4769 castalia. *Celestial Mechanics and Dynamical Astronomy*, 65:313–344, 1997.

[7] A. Colagrossi, F. Ferrari, M. Lavagna, and K. Howell. Dynamical evolution about asteroids with high fidelity gravity field and perturbations modeling. In J.D. Turner, G.G. Wawrzyniak, W.T. Cerven, and M. Majji, editors, *Advances in the Astronautical Sciences (Proceedings of the AIAA/AAS Astrodynamics Specialist Conference)*, volume 156, pages 885–903, Napa, CA, USA, 2016. Univelt Inc.

[8] A Colagrossi, F Ferrari, and M Lavagna. Coupled dynamics analysis around asteroids by

means of accurate shape and perturbations modeling. In *Proceedings of the 66th International Astronautical Congress*, Jerusalem, IS, 2015.

[9] F Ferrari, A Tasora, P Masarati, and M Lavagna. Numerical simulation of n-body asteroid aggregation. In *Multibody Dynamics, Josep M. Font-Llagunes (Ed.)*, pages 936–947, Barcelona, ES, 2015.

[10] Yang Yu, Patrick Michel, Stephen R Schwartz, Shantanu P Naidu, and Lance AM Benner. Ejecta cloud from the aida space project kinetic impact on the secondary of a binary asteroid: I. mechanical environment and dynamical model. *Icarus*, 282:313–325, 2017.

[11] Kevin R Housen and Keith A Holsapple. Ejecta from impact craters. *Icarus*, 211(1):856–875, 2011.

[12] AM Stickle, JA Atchison, OS Barnouin, AF Cheng, DA Crawford, CM Ernst, Z Fletcher, and AS Rivkin. Modeling momentum transfer from kinetic impacts: Implications for redirecting asteroids. *Procedia Engineering*, 103:577–584, 2015.